Electromagnetics, 26:3–35, 2006

ISSN: 0272-6343 print/1532-527X online
DOI: 10.1080/02726340500214894

Taylor & Francis
Taylor & Francis Group

Statistics of Impedance and Scattering Matrices in Chaotic Microwave Cavities: Single Channel Case

XING ZHENG

Department of Physics
and Institute for Research in Electronics and Applied Physics
University of Maryland
College Park, Maryland, USA

THOMAS M. ANTONSEN JR.
EDWARD OTT

Department of Physics
and Institute for Research in Electronics and Applied Physics
and Department of Electrical and Computer Engineering
University of Maryland
College Park, Maryland, USA

We study the statistical properties of the impedance (Z) and scattering (S) matrices of open electromagnetic cavities with several transmission lines or waveguides connected to the cavity. In this paper, we mainly discuss the single port case. The generalization to multiple ports is treated in a companion paper. The model we consider is based on assumed properties of chaotic eigenfunctions for the closed system. Analysis of the model successfully reproduces features of the random matrix model believed to be universal, while at the same time incorporating features which are specific to individual systems as treated by the Poisson kernel of Mello et al. Statistical properties of the cavity impedance Z are obtained in terms of the radiation impedance (i.e., the impedance seen at a port with the cavity walls moved to infinity). Effects of wall absorption are discussed. Theoretical predictions are tested by direct comparison with numerical solutions for a specific system. (Here the word universal is used to denote high frequency statistical properties that are shared by the members of the general class of systems whose corresponding ray trajectories are chaotic. These universal properties are, by definition, independent of system-specific details.)

Keywords wave chaos, impedance, scattering matrix

Received 18 June 2004; accepted 22 February 2005.

We thank R. E. Prange, S. Fishman, J. Rogers, and S. Anlage for discussions and help. This work was supported in part by the DOD MURI for the study of microwave effects under AFOSR Grant F496200110374.

Address correspondence to Dr. Xing Zheng, Institute for Research in Electronics and Applied Physics, University of Maryland, College Park, MD, 20742, USA. E-mail: plzhengx@Glue.umd.edu

Introduction

The problem of the coupling of electromagnetic radiation in and out of structures is a general one which finds applications in a variety of scientific and engineering contexts. Examples include the susceptibility of circuits to electromagnetic interference, the confinement of radiation to enclosures, as well as the coupling of radiation to structures used to accelerate charged particles.

Because of the wave nature of radiation, the coupling properties of a structure depend in detail on the size and shape of the structure, as well as the frequency of the radiation. In considerations of irregularly shaped electromagnetic enclosures for which the wavelength is fairly small compared with the size of the enclosure, it is typical that the electromagnetic field pattern within the enclosure, as well as the response to external inputs, can be very sensitive to small changes in frequency and to small changes in the configuration. Thus, knowledge of the response of one configuration of the enclosure may not be useful in predicting that of a nearly identical enclosure. This motivates a statistical approach to the electromagnetic problem.

While our ability to numerically compute the response of particular structures has advanced greatly in recent years, the kind of information needed for a statistical description may not be obtainable directly from numerical computation.

Thus it would seem to be desirable to have specific analytical predictions for the statistics of electromagnetic quantities in such circumstances. This general problem has received much attention in previous work (e.g., Holland & St. John, 1994, 1999; Lehman & Miller, 1991; Kostas & Boverie, 1991; Price, Davis, & Wenaas, 1993; Hill, 1994; Barthélemy, Legrand, & Mortessagne, 2004). Some of the main issues addressed are: the probability distribution of fields at a point, the correlation function of fields at two points near each other, the statistics of the excitation of currents in cables or in small devices within the enclosure, the cavity Q, the statistics of coupling to the enclosure, and the statistics of scattering properties. A fundamental basis for most of these studies is that, due to the complexity of the enclosure and the smallness of the wavelength compared to the enclosure size, the electromagnetic fields approximately obey a statistical condition that we shall call *the random plane wave hypothesis*, which assumes that a superposition of random plane wave can be used to describe the statistics of chaotic wave functions (Berry, 1983). This work has been quite successful in obtaining meaningful predictions, and some of these have been tested against experiments with favorable results. A good introduction and overview is provided in the book by Holland and St. John (1999).

In addition to this previous work on *statistical electromagnetics* (Holland & St. John, 1994, 1999; Lehman & Miller, 1991; Kostas & Boverie, 1991; Price, Davis, & Wenaas, 1993; Hill, 1994; Barthélemy, Legrand, & Mortessagne, 2004), much related work has been done by theoretical physicists. The physicists are interested in solutions of quantum mechanical wave equations when the quantum mechanical wavelength is short compared with the size of the object considered. Even though the concern is not electromagnetics, the questions addressed and the results are directly applicable to wave equations in general and to electromagnetics in particular. The start of this line of inquiry was a paper by Eugene Wigner (1955). Wigner's interest was in the energy levels of large nuclei. Since the energy level density at high energy is rather dense, and since the solution of the wave equations for the levels was inaccessible, Wigner proposed to ask statistical questions about the levels. Wigner's results apply directly to the statistics of resonant frequencies in highly overmoded irregularly shaped electromagnetic cavities. Since Wigner's work, and especially in recent years, the statistical approach to wave equations has been a very

active area in theoretical physics, where the field has been called "quantum chaos." We emphasize, however, that the quantum aspect to this work is not inherent and that a better terminology, emphasizing the generality of the issues addressed, might be "wave chaos." For a review, see chapter 11 of Ott (2002) or the books by Gutzwiller (1990) or Haake (1991).

Wigner's approach was to introduce what is now called Random Matrix Theory (RMT) (Mehta, 1991). In RMT the linear wave equation is replaced or modelled by a linear matrix equation where the elements of the matrix are random variables. This follows from Wigner's hypothesis that the eigenvalues for a complicated (in our case chaotic) system have the same statistics as those of matrices drawn from a suitable ensemble. Based on symmetry arguments, Wigner proposed that the matrix statistics are those that would result if the matrix were drawn from different types of ensembles, where the relevant ensemble type depends only on gross symmetries of the modelled system. The two ensembles that are relevant to electromagnetic problems are the Gaussian Orthogonal Ensemble (GOE) and the Gaussian Unitary Ensemble (GUE). In both cases, all the matrix elements are zero mean Gaussian random variables. In the GOE all the diagonal element distributions have the same width, while all the off-diagonal element distributions have widths that are half that of the diagonal elements. The matrices are constrained to be symmetric, but otherwise the elements are statistically independent. The GOE case is intended to model wave systems that have time reversal symmetry (TRS). That is, the time domain equations are invariant under the transformation $t \to -t$. This is the case for electromagnetic waves if the permittivities and permeabilities tensors are real and symmetric. In the GUE the matrices are constrained to be *Hermitian*. In this case the off-diagonal elements are complex and the distributions of their real and imaginary parts are independent and Gaussian and the width of these Gaussians is again one half the width of the real diagonal elements. The GUE case is intended to model systems for which time reversal symmetry is broken (TRSB). This case will apply in electromagnetics if a nonreciprocal element such as a magnetized ferrite or a cold magnetized plasma is added to the system.

In this paper we mainly consider an irregularly shaped cavity with a single transmission line and/or waveguide connected to it, and we attempt to obtain the statistical properties of the impedance Z and the scattering matrix S (which are both scalars in the cases we consider) characterizing the response of the cavity to excitations from the connected transmission line, where the wavelength is small compared to the size of the cavity. We will treat specifically the case of cavities that are thin in the vertical (z-direction) direction. In this case the resonant fields of the closed cavity are transverse electromagnetic (TM_z, $\vec{E} = E_z(x, y)\hat{z}$), and the problem admits a purely scalar formulation. While the two-dimensional problem has practical interest in appropriate situations (e.g., the high frequency behavior of the power plane of a printed circuit), we emphasize that the results for the statistical properties of Z and S matrices are predicted to apply equally well to three-dimensional electromagnetics and polarized waves. We note that previous work on statistical electromagnetics (Holland & St. John, 1994, 1999; Lehman & Miller, 1991; Kostas & Boverie, 1991; Price, Davis, & Wenaas, 1993; Hill, 1994; Barthélemy, Legrand, & Mortessagne, 2004) is for fully three-dimensional situations. Our main motivation for restricting our considerations here to two dimensions is that it makes possible direct numerical tests of our predictions (such numerical predictions might be problematic in three dimensions due to limitations on computer capabilities). Another benefit is that analytical work and notation are simplified.

For an electrical circuit or electromagnetic cavity with ports, the impedance matrix provides a characterization of the structure in terms of the linear relation between the voltages and currents at all ports,

$$\hat{V} = Z\hat{I}, \tag{1}$$

where $\hat{V}$ and $\hat{I}$ are column vectors of the complex phasor amplitudes of the sinusoidal port voltages and currents. The scattering matrix S is related to the impedance matrix Z by

$$S = Z_0^{1/2}(Z + Z_0)^{-1}(Z - Z_0)Z_0^{-1/2}, \tag{2}$$

where Z_0 is the characteristic impedance of the transmission line.

As discussed in the next section, the impedance matrix Z can be expressed in terms of the eigenfunctions and eigenvalues of the closed cavity. We will argue that the elements of the Z matrix can be represented as combinations of random variables with statistics based on the random plane wave hypothesis for the representation of chaotic wave functions and results from random matrix theory (Wigner, 1951; Ott, 2002) for the distribution of the eigenvalues.

This approach to determination of the statistical properties of the Z and S matrices allows one to include the generic properties of these matrices, as would be predicted by representing the system as a random matrix drawn from an appropriate ensemble. It also, however, allows one to treat aspects of the S and Z matrices which are specific to the problems under consideration (i.e., so-called *nonuniversal* properties).

These nonuniversal properties have previously been treated within the context of the so-called Poisson Kernel based on a "maximum information entropy" principle (Mello, Peveyra, & Seligman, 1985), and Brouwer (1995) later provided a microscopic justification and showed that the Poisson Kernel can be derived from Wigner's RMT description of the Hamilton. Here the statistics of the S matrix depend in a nontrivial way on the average of S taken in a narrow frequency range. This characterizes the system-specific aspects of the coupling. Our approach allows one to *predict* the average based on another informative quantity, the radiation impedance, which itself characterizes the coupling of the port to the enclosure. The radiation impedance is the impedance that applies at the port when waves are launched into the cavity and (by making the distant walls perfectly absorbing) not allowed to return. Our interpretation of the role of the radiation impedance is equivalent to Brouwer's (1995) interpretation of the Poisson kernel in terms of scattering from a cascaded configuration of a lossless multiport and a perfectly coupled cavity described by RMT. We show that the separation of universal and system-specific properties is more natural when considering the impedance rather than scattering matrix. Specifically, the universal properties of the cavity impedance are observed by subtracting from the raw cavity impedance the radiation reactance and normalizing the result to the radiation resistance. The statistics of the resulting variable, which we term the normalized cavity impedance, depend only on a single parameter characterizing the internal loss of the cavity.

The Poisson kernel description of the scattering amplitude has been applied to data obtained from microwave scattering experiments on cavities with absorption (Doron & Smilansky, 1990; Méndez-Sánchez et al., 2003; Kuhl et al.). Two different methods have recently been described (Méndez-Sánchez et al., 2003; Kuhl et al.) for extracting the universal properties of the scattering amplitude from the system-specific ones.

The system-specific properties are characterized in terms of averages of the scattering amplitude and its modulus squared over ranges of frequency. A fitting procedure is then used to characterize the universal fluctuations. The impedance approach has also been applied to experimental data (Warne et al., 2003; Hemmady et al., 2004). In Hemmady et al. (2004) the radiation impedance is measured directly and the complex normalized impedance is formed by subtracting the radiation reactance and normalizing to the radiation resistance. The probability distribution function of the normalized impedance was then compared directly with Monte Carlo numerical evaluations of the prediction.

The main contribution of this paper is to describe the statistical properties of the cavity impedance. First we show (also shown in Warne et al. (2003)) that the relation between the cavity impedance and the radiation impedance follows from the assumption that the eigenfunctions of the cavity satisfy the random plane wave hypothesis of Berry (1983). We then verify the relation between the cavity impedance and the radiation impedance for a specific realization by numerical simulation using the High Frequency Structure Simulation software (HFSS). Next, using Monte Carlo methods we evaluate theoretical predictions for the probability distribution functions for the real and imaginary parts of the normalized impedance for different values of internal absorption in the cavity. The distribution of the real part of the normalized impedance is closely related to the distribution of values that is known as the local density of states (Efetov & Prigodin, 1993). Finally, we derive expressions for the mean and variance of the normalized impedance as functions of the level of internal loss in the cavity.

Our paper is organized as follows. We first present the statistical model. We then illustrate our model by application to the statistics of the impedance seen at a single transmission line input to a cavity that is irregularly shaped, highly overmoded, lossless, and nongyrotropic (i.e., no magnetized ferrite). We then relate the impedance matrix characteristics to those of the scattering matrix and generalize our model to incorporate the effects of distributed loss (such as wall absorption). Throughout, our analytical results will be compared with direct numerical solutions of the wave problem. We conclude with a discussion and summary of results.

Modelling with Random Plane Waves

We consider a closed cavity with ports connected to it. For specificity, in our numerical work, we consider the particular, but representative, example of the vertically thin cavity shown in Figure 1a coupled to the outside via a coaxial transmission cable. Figure 1b shows an example of how this cavity might be connected to a transmission line via a hole in the bottom plate. The cavity shape in Figure 1 is of interest here because the concave curvature of the walls insures that typical ray trajectories in the cavity are chaotic. (Figure 1a is a quarter of the billiard shown in Figure 2c.) For our purposes, a key consequence of the chaotic property of the shape in Figure 1a is that, if we consider the trajectory of a particle bouncing with specular reflection at the walls (equivalently a ray path), then a randomly chosen initial condition (i.e., random in position $\vec{x}$ within the cavity and isotropically random in the orientation θ of the initial velocity vector) always generates an orbit that is *ergodic* within the cavity. Here by ergodic we mean the following: For any spatial region R within the cavity, in the limit of time $t \to \infty$, the fraction of time the orbit spends in R is the ratio of the area of R to the entire area of the two-dimensional cavity, and, furthermore, the collection of velocity orientations θ of the orbit when it is in R generates a uniform distribution in $[0, 2\pi)$. Thus the orbit *uniformly* covers the phase space $(\vec{x}, \theta)$. This is to be contrasted with the case of a rectangular

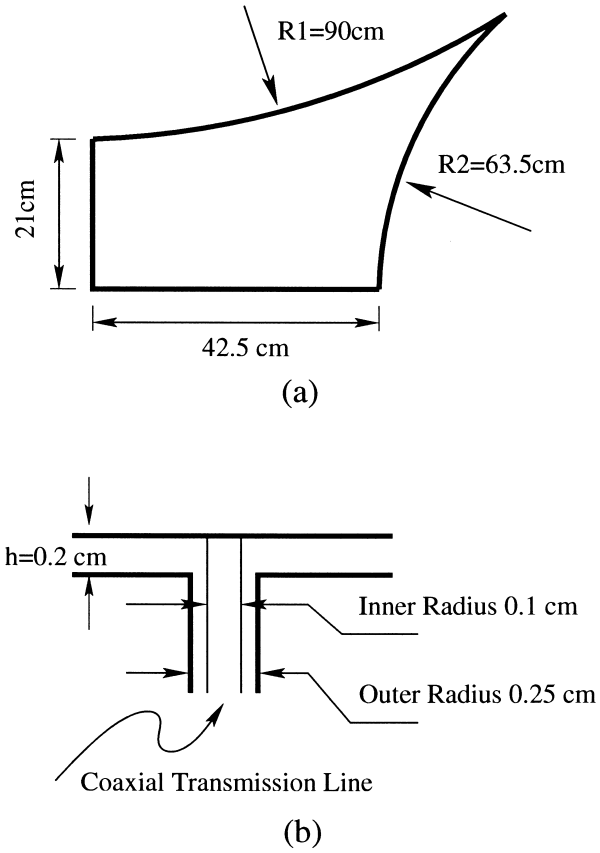

Figure 1. (a) Top view of the cavity used in our numerical simulation. (b) Side view of the details of a possible coupling.

cavity, $0 \leq x \leq a$, $0 \leq y \leq b$, which represents a shape for which orbits (rays) are nonchaotic. In that case, if the initial velocity orientation with respect to the x-axis is θ_0, then at any subsequent time only four values of θ are possible: θ_0, $2\pi - \theta_0$, $\pi - \theta_0$, $\pi + \theta_0$. In cases such as Figure 1a we assume that the previously mentioned hypotheses regarding eigenfunctions and eigenvalue distributions provide a useful basis for deducing the statistical properties of the Z and S matrices, and, in what follows, we investigate and test the consequences of this assumption.

The vertical height h of the cavity is small, so that, for frequencies of interest, the only propagating waves inside the cavity have electric fields that are purely vertical,

$$\vec{E} = E_z(x, y)\hat{z}. \tag{3}$$

This electric field gives rise to a charge density on the top plate $\rho_s = -\epsilon_0 E_z$, and also generates a voltage $V_T(x, y) = -hE_z(x, y)$ between the plates. The magnetic field is perpendicular to $\hat{z}$,

$$\vec{B} = (B_x, B_y) = \mu_0 \vec{H}, \tag{4}$$

and is associated with a surface current density $\vec{J}_s = \vec{H} \times \hat{z}$ flowing on the top plate.

The cavity excitation problem for a geometry like that in Figure 1b is system specific. We will be interested in separating out statistical properties that are independent of the coupling geometry and have a universal (i.e., system-independent) character. For this purpose, we claim that it suffices to consider a simple solvable excitation problem, and then generalize to more complicated cases, such as the coupling geometry in Figure 1b. Thus we consider the closed cavity (i.e., with no losses or added metal), with localized current sources resulting in a current density $\vec{J}_s(x, y, t) = \sum_i I_i(t)u_i(x, y)\hat{z}$ between the plates. The profile functions $u_i(x, y)$ are assumed to be localized; i.e., $u_i(x, y)$ is essentially zero for $(x - x_i)^2 + (y - y_i)^2 > l_i^2$, where l_i is much smaller than the lateral cavity dimension. $u_i(x, y)$ characterizes the distribution of vertical current at the location of the ith model input (analogous to the ith transmission line connected to the cavity, although, for this model, there are no holes in the upper or lower plates). The profile is normalized such that

$$\int dxdyu_i(x, y) = 1. \tag{5}$$

For the sake of simplicity, we only consider the single port case in this paper (i.e., there is only one localized source and we may thus drop the subscript i on $u_i(x, y)$). The injection of current serves as a source in the continuity equation for surface charge, $\partial\rho_s/\partial t + \nabla \cdot \vec{J}_s = Iu(x, y)$, where $\nabla = (\partial/\partial x, \partial/\partial y)$. Expressed in terms of fields, the continuity equation becomes

$$\frac{\partial}{\partial t}(-\epsilon_0 E_z) + \nabla \cdot (\tilde{H} \times \hat{z}) = Iu(x, y). \tag{6}$$

Differentiating Eq. (6) with respect to t and using Faraday's law, we obtain

$$\frac{\partial^2}{\partial t^2}(-\epsilon_0 E_z) + \nabla \cdot \frac{1}{\mu_0}\nabla E_z = u(x, y)\frac{\partial I}{\partial t}. \tag{7}$$

Expressing the electric field in terms of the voltage $V_T = -E_z h$, we arrive at the driven wave equation

$$\frac{1}{c^2}\frac{\partial^2}{\partial t^2}V_T - \nabla^2 V_T = h\mu_0 u\frac{\partial I}{\partial t}, \tag{8}$$

where c is speed of light, $c^2 = 1/(\mu_0\epsilon_0)$.

Assuming sinusoidal time dependence $e^{j\omega t}$ for all field quantities, we obtain the following equation relating $\hat{V}_T$ and $\hat{I}$, the phasor amplitudes of the voltage between the plates and the port current:

$$(\nabla^2 + k^2)\hat{V}_T = -j\omega h\mu_0 u\hat{I} = -jkh\eta_0 u\hat{I}, \tag{9}$$

where $\eta_0 = \sqrt{\mu_0/\epsilon_0}$ is the characteristic impedance of free space and $k = \omega/c$. Thus Eq. (9) represents a wave equation for the voltage between the plates excited by the input current.

To complete our description and arrive at an expression of the form of Eq. (1), we need to determine the port voltage V. We take its definition to be a weighted average of the spatially dependent voltage $V_T(x, y, t)$,

$$V = \int dxdyu(x, y)V_T(x, y, t). \tag{10}$$

This definition is chosen because it then follows from Eq. (6) that the product IV gives the rate of change of field energy in the cavity, and thus Eq. (10) provides a reasonable definition of port voltage. Solution of Eq. (9) and application of (10) to the complex phasor amplitude $\hat{V}_T$ provide a linear relation between $\hat{V}$ and $\hat{I}$, which defines the impedance Z.

To solve Eq. (9), we expand $\hat{V}_T$ in the basis of the eigenfunctions of the closed cavity, i.e., $\hat{V}_T = \sum_n c_n \phi_n$, where $(\nabla^2 + k_n^2)\phi_n = 0$, $\int \phi_i \phi_j dx dy = \delta_{ij}$, and $\phi_n(x, y) = 0$ at the cavity boundary. Thus, multiplying Eq. (9) by ϕ_n and integrating over (x, y) yields

$$c_n(k^2 - k_n^2) = -jkh\eta_0 \langle u\phi_n \rangle \hat{I}, \tag{11}$$

where $k_n = \omega_n/c$, ω_n is the eigenfrequency associated with ϕ_n, and $\langle u\phi_n \rangle = \int \phi_n u dx dy$. Solving for the coefficients c_n and computing the voltage $\hat{V}$ yields

$$\hat{V} = -j \sum_n \frac{kh\eta_0 \langle u\phi_n \rangle^2}{k^2 - k_n^2} \hat{I} = Z\hat{I}. \tag{12}$$

This equation describes the linear relation between the port voltage and the current flowing into the port. Since we have assumed no energy dissipation so far (e.g., due to wall absorption or radiation), the impedance of the cavity is purely imaginary, as is indicated by Eq. (12).

The expression for Z in Eq. (12) is equivalent to a formulation introduced by Wigner and Eisenbud (1947) in nuclear-reaction theory in 1947, which was generalized and reviewed by Lane and Thomas (1958), and Mahaux and Weidenmüller (1996). Recently, a supersymmetry approach to scattering based on this formulation was introduced by Verbaarschot, Weidenmüller, and Zirnbauer (1985) and further developed by Lewenkopf and Weidenmüller (1991) and Fyodorov and Sommers (1997) (which they called the "K-matrix" formalism) and it has also been adapted to quantum dots by Jalabert, Stone, and Alhassid (1992).

Explicit evaluation of Eq. (12) in principle requires determination of the eigenvalues and corresponding eigenfunctions of the closed cavity. We do not propose to do this. Rather, we adopt a statistical approach to replace $\langle u\phi_n \rangle$ and k_n^2 with random variables with appropriate distribution, such that we can construct models for the statistical behavior of the impedance. For high frequencies such that $k = \omega/c \gg L^{-1}$, where L is a typical dimension of the cavity, the sum in Eq. (12) will be dominated by high order (short wavelength) modes with $k_n L \gg 1$, and the properties of the short wavelength eigenfunctions can be understood in terms of ray trajectories. For geometries like that in Figure 1a, ray trajectories are chaotic.

The assumed form of the eigenfunction from the random plane wave hypothesis is

$$\phi_n = \lim_{N\to\infty} \sqrt{\frac{2}{AN}} \mathrm{Re} \left\{ \sum_{i=1}^{N} \alpha_i \exp(jk_n \vec{e}_i \cdot \vec{x} + j\theta_i) \right\}, \tag{13}$$

where $\vec{e}_i$ are randomly oriented unit vectors (in the x-y plane), θ_i is random in $[0, 2\pi]$, and α_i are random. This statistical model for ϕ_n is motivated by the previously discussed ergodicity of ray paths in chaotic cavities (e.g., Figure 1a); i.e., the random orientation of $\vec{e}_i$ corresponds to the uniform distribution of ray orientations θ. Using (13) we can calculate the overlap integral $\langle u\phi_n \rangle$ appearing in the numerator of (12). Being the sum of contributions from a large number of random plane waves, the central limit theorem

implies that the overlap integral will be a Gaussian random variable with zero mean. The variance of the overlap integral can be obtained using Eq. (13):

$$E\{\langle u\phi_n\rangle^2\} = \frac{1}{A}\int_0^{2\pi}\frac{d\theta}{2\pi}|\bar{u}(\vec{k}_n)|^2, \tag{14}$$

where $E\{.\}$ denotes the expected value, $\bar{u}(\vec{k}_n)$ is the Fourier transform of the profile function $u(x, y)$,

$$\bar{u}(\vec{k}_n) = \int dxdyu(x, y)\exp(-j\vec{k}_n\cdot\vec{x}), \tag{15}$$

and $\vec{k}_n = (k_n\cos\theta, k_n\sin\theta)$. The integral in (14) over θ represents averaging over the directions $\vec{e_j}$ of the plane waves. The variance of $\langle u\phi_n\rangle$ depends on the eigenvalue k_n^2. If we consider a localized source $u(x, y)$ such that the size of the source is less than the typical wavelength $2\pi/k_n$, then the variance will be A^{-1} (recall the normalization of u given by Eq. (5)).

Modelling of Eq. (12) also requires specifying the distribution of eigenvalues k_n appearing in the denominator. According to the Weyl formula (Ott, 2002), for a two-dimensional cavity of area A, the average separation between adjacent eigenvalues, $k_n^2 - k_{n-1}^2$, is $4\pi A^{-1}$. Thus, one requirement of the sequence of eigenvalues is that they have a mean spacing $4\pi A^{-1}$. The distribution of spacings of adjacent eigenvalues is predicted to have the characteristic Wigner form for cavities with chaotic trajectories. In particular, defining the normalized spacing, $s_n = A(k_n^2 - k_{n-1}^2)/4\pi$, it is found that there are two basic cases which (for reasons explained subsequently) are called "time reversal symmetric" (TRS) and "time-reversal symmetry broken" (TRSB). The probability density function for s_n is predicted to be closely approximated by

$$P(s_n) = \frac{\pi}{2}s_n\exp(-\pi s_n^2/4) \tag{16}$$

for chaotic systems with TRS and

$$P(s_n) = \frac{32}{\pi}s_n^2\exp(-4s_n^2/\pi) \tag{17}$$

for the TRSB system. Thus, a second requirement on the sequence of eigenvalues is that they have the correct spacing distribution. The TRS case applies to systems where the permittivity and permeability tensors are real and diagonal. The TRSB case applies to systems where the permittivity or permeability tensors are complex but hermitian, as they are for a magnetized ferrite.

One approach of ours will be to generate values for the impedance assuming that sequences of eigenvalues can be generated from a set of separations s_n which are independent and distributed according to Eq. (16). The usefulness of the assumption of the independence of separations will have to be tested, as it is known that there are long range correlations in the spectrum, even if nearby eigenvalues appear to have independent spacings. A more complete approach is to use a sequence of eigenvalues taken from the spectra of random matrices. When this is done the impedance defined in Eq. (12) (with independent Gaussian distributions for the overlap integrals) is completely equivalent to that obtained in RMT. We will find that in some cases it is sufficient to consider the simpler spectra, generated from independent spacing distributions, but in other cases,

for example, when losses are considered or when correlations of impedance values at different frequencies are considered, the correlations in eigenvalues exhibited by random matrix theory are important. This will be discussed more thoroughly later in the paper.

A key assumption in our model is the statistical independence of the overlap integrals, $\langle u\phi_n \rangle$, and the eigenvalues k_n. This we argue on the basis that each eigenfunction satisfies the plane wave hypothesis and successive eigenfunctions appear to be independent. A second justification comes from random matrix theory where it is known that the probability distribution for the eigenvalues of a random matrix is independent of that of the elements of the eigenfunctions (Mehta, 1991, chap. 3). Indeed, the result from the random plane wave hypothesis (Eq. (18), below) turns out to be equivalent to past work on scattering matrices that was based on coupling to systems described by random matrix theory (Mello, Peveyra, & Seligman, 1985).

Combining our expressions for $\langle u\phi_n \rangle$ and using the result that for a two-dimensional cavity the mean spacing between adjacent eigenvalues is $\Delta = 4\pi A^{-1}$, the expression for the cavity impedance given in Eq. (12) can be rewritten,

$$Z = -\frac{j}{\pi} \sum_{n=1}^{\infty} \Delta \frac{R_R(k_n) w_n^2}{k^2 - k_n^2}, \tag{18}$$

where w_n is taken to be a Gaussian random variable with zero mean and unit variance, the k_n are distributed independent of the w_n, and R_R is given by

$$R_R(k) = \frac{kh\eta_0}{4} \int \frac{d\theta}{2\pi} |u(\vec{k})|^2. \tag{19}$$

Our rationale for expressing the impedance in the form of Eq. (18) and introducing $R_R(k_n)$ is motivated by the following observation. Suppose we allow the lateral boundaries of the cavity to be moved infinitely far from the port. That is, we consider the port as a two-dimensional free-space radiator. In this case, we solve Eq. (9) with a boundary condition corresponding to outgoing waves, which can be readily done by the introduction of Fourier transforms. This allows us to compute the phasor port voltage $\hat{V}$ by Eq. (10). Introducing a complex radiation impedance $Z_R(k) = \hat{V}/\hat{I}$ (for the problem with the lateral boundaries removed), we have

$$Z_R(k) = -\frac{j}{\pi} \int_0^{\infty} \frac{dk_n^2}{k^2 - k_n^2} R_R(k_n), \tag{20}$$

where $R_R(k_n)$ is given by Eq. (19) and k_n is now a continuous variable. The impedance $Z_R(k)$ is complex with a real part obtained by deforming the k_n integration contour to pass above the pole at $k_n = k$. This follows as a consequence of applying the outgoing wave boundary condition, or equivalently, letting k have a small negative imaginary part. Thus, we can identify the quantity $R_R(k)$ in Eq. (19) as the radiation resistance of the port resulting from one half the residue of the integral in (20) at the pole, $k_n^2 = k_n$,

$$\mathrm{Re}[Z_R(k)] = R_R(k), \tag{21}$$

and

$$X_R(k) = \mathrm{Im}[Z_R(k)]$$

is the radiation reactance given by the principal part (denoted by P) of the integral (20),

$$X_R(k) = P\left\{-\frac{1}{\pi}\int_0^\infty \frac{dk_n^2}{k^2 - k_n^2} R_R(k_n)\right\}. \tag{22}$$

Based on the above, the connection between the cavity impedance, represented by the sum in Eq. (18), and the radiation impedance, represented in Eq. (21) and Eq. (22), is as follows. The cavity impedance, Eq. (18), consists of a discrete sum over eigenvalues k_n with weighting coefficients w_n which are Gaussian random variables. There is an additional weighting factor $R_R(k_n)$ in the sum, which is the radiation resistance. The radiation reactance, Eq. (22), has a form analogous to the cavity impedance. It is the principle part of a continous integral over k_n with random coupling weights set to unity. While, Eqs. (18), (21), (22), have been obtained for the simple model input $\hat{J} = \hat{I}u(x, y)$ in $0 \le z \le h$ with perfectly conducting plane surfaces at $z = 0, h$, we claim that these results apply in general. That is, for a case like that in Figure 1b, $Z_R(k)$ (which for the simple model is given by Eq. (20)) can be replaced by the radiation impedance for the problem with the same port geometry. We also note that while (20) was obtained with reference to a two-dimensional problem, the derivation and result are the same in three dimensions. It is important to note that, while $R_R(k)$ is nonuniversal (i.e., depends on the specific coupling geometry, such as that in Figure 2b), it is sometimes possible to independently calculate it, and it is also a quantity that can be directly measured (e.g., an experimental radiation condition can be simulated by placing the absorber adjacent to the lateral walls). In the next section, we will use the radiation impedance to normalize the cavity impedance, yielding a universal distribution for the impedance of a chaotic cavity.

Impedance Statistics for a Lossless, Time Reversal Symmetric Cavity

In the lossless case, the impedance of the cavity Z in Eq. (18) is a purely imaginary number and S, the reflection coefficient, is a complex number with unit modulus. Terms in the summation of Eq. (18) for which k^2 is close to k_n^2 will give rise to large fluctuations in Z as either k^2 is varied or one considers different realizations of the random numbers. The terms for which k^2 is far from k_n^2 will contribute to a mean value of Z. Accordingly, we write

$$Z = \bar{Z} + \tilde{Z}, \tag{23}$$

where $\bar{Z}$, the mean value of Z, is written as

$$\bar{Z} = -\frac{j}{\pi}\sum_n \Delta E\left\{\frac{R_R(k_n^2)}{k^2 - k_n^2}\right\}, \tag{24}$$

and we have used the fact that the w_n^2 are independent with $E\{w_n^2\} = 1$. If we approximate the summation in Eq. (24) by an integral, noting that Δ is the mean spacing between eigenvalues, comparison with (22) yields

$$\bar{Z} = jX_R(k), \tag{25}$$

where $X_R = \mathrm{Im}[Z_R]$ is the radiation reactance defined by Eq. (22). Thus, the mean part of the fluctuating impedance of a closed cavity is equal to the radiation reactance that

would be obtained under the same coupling conditions for an antenna radiating freely; i.e., in the absence of multiple reflections of waves from the lateral boundaries of the cavity. The equivalent conclusion for the radiation scattering coefficient is evident from the treatment of Brouwer (1995).

We now argue that, if k^2 is large enough that many terms in the sum defining Z satisfy $k_n^2 < k^2$, then the fluctuating part of the impedance $\tilde{Z}$ has a Lorentzian distribution with a characteristic width $R_R(k)$. That is, we can write

$$Z = j(X_R + R_R\xi), \tag{26}$$

where ξ is a zero mean unit width Lorentzian distributed random variable, $P_\xi(\xi) = [\pi(1+\xi^2)]^{-1}$.

Lorentzian distribution appears in the theory of nuclear scattering (Krieger, 1967) and arises as consequences of random matrix theory (Fyodorov & Sommers, 1997; Mello, 1995). That the characteristic width scales as $R_R(k)$ follows from the fact that the fluctuating part of the impedance is dominated by terms for which $k_n^2 \simeq k^2$. The size of the contribution of a term in the sum in Eq. (18) decreases as $|k^2 - k_n^2|$ in the denominator increases. The many terms with large values of $|k^2 - k_n^2|$ contribute mainly to the mean part of the reactance, with the fluctuations in these terms cancelling one another due to the large number of such terms. The contributions to the mean part from the relatively fewer terms with small values of $|k^2 - k_n^2|$ tend to cancel due to the sign change of the denominator while their contribution to the fluctuating part of the reactance is significant since there are a smaller number of these terms. Consequently, when considering impedance fluctuations, it suffices to treat $R_R(k_n)$ as a constant in the summation in Eq. (18) and factor it out. This results in a sum that is independent of coupling geometry and is therefore expected to have a universal distribution.

Numerical Results for a Model Normalized Impedance

To test the arguments above, we consider a model normalized cavity reactance $\tilde{\xi} = X/R_R$ and also introduce a normalized wavenumber $\tilde{k}^2 = k^2/\Delta = k^2 A/4\pi$. In terms of this normalized wavenumber, the average of the eigenvalue spacing [average of $(\tilde{k}_{n+1}^2 - \tilde{k}_n^2)$] is unity. Our model normalized reactance is

$$\tilde{\xi} = -\frac{1}{\pi}\sum_{n=1}^{N}\frac{w_n^2}{\tilde{k}^2 - \tilde{k}_n^2}, \tag{27}$$

where the w_n are independent Gaussian random variables, $\tilde{k}_n^2$ are chosen according to various distributions, and we have set $R_R(k_n)$ to a constant value for $n \le N$ and $R_R(k_n) = 0$ for $n > N$. The fluctuating part of $j\xi$ given by Eq. (27) mimics the fluctuating part of the impedance Z in the case in which $R_R(k_n)$ has a sharp cut-off for eigenmodes with $n > N$. In terms of ξ, Eq. (26) becomes

$$P_{\tilde{\xi}}(\tilde{\xi}) = \frac{1}{\pi}\frac{1}{[(\tilde{\xi} - \bar{\xi})^2 + 1]}, \tag{28}$$

where $\bar{\xi}$ is the mean of ξ.

First we consider the hypothetical case where the collection of $\tilde{k}_n^2$ values used in Eq. (27) result from N independent and uniformly distributed random choices in the

interval $0 \leqslant \tilde{k}_n^2 \leqslant N$. In contrast to Eqs. (16), this corresponds to a Poisson distribution of spacings $P(s) = \exp(-s)$ for large N. This case is analytically solvable (Mello, 1995) and the mean value $\bar{\xi}$ is

$$\bar{\xi} = P\left\{-\frac{1}{\pi}\int_0^N \frac{d\tilde{k}_n^2}{\tilde{k}^2 - \tilde{k}_n^2}\right\} = \frac{1}{\pi}\ln\left|\frac{N-\tilde{k}^2}{\tilde{k}^2}\right|; \tag{29}$$

furthermore, ξ has a Lorentzian distribution given by Eq. (28).

Our next step is to numerically determine the probability distribution function for ξ given by (27) in the case where the spacing distribution corresponds to the TRS case described by Eq. (3). We generated 10^6 realizations of the sum in Eq. (27). For each realization we randomly generated $N = 2000$ eigenvalues using the spacing probability distribution (3), as well as $N = 2000$ random values of w_n chosen using a Gaussian distribution for w_n with $E\{w_n\} = 0$ and $E\{w_n^2\} = 1$. We first test the prediction of Eq. (29) by plotting the median value of ξ versus $\tilde{k}^2$ in Figure 2a. (We use the median rather than the mean, since, for a random variable with a Lorentzian distribution, this quantity is more robust when a finite sample size is considered.) Also plotted in Figure 2a is the formula (29). We see that the agreement is very good. Next we test the prediction for the fluctuations in ξ by plotting a histogram of ξ values for the case $\tilde{k}^2 = N/2$ in Figure 2b. From (29) for $\tilde{k}^2 = N/2$ the mean is expected to be zero and, as can be seen in the figure, the histogram (open circles) corresponds to a Lorentzian with zero mean and unit width (solid line) as expected. Histograms plotted for other values of $\tilde{k}^2$ agree with the prediction but are not shown. Thus, we find that the statistics of ξ are the same for $P(s) = \exp(-s)$ (Poisson) and for $P(s)$ given by Eq. (16). Hence we conclude that the statistics of ξ are independent of the distribution of spacings. This is further supported by Figure 2c, where the histogram of ξ for $\tilde{k}^2 = N/2$ is plotted for the case in which the spacing distribution is that corresponding to TRSB systems (the TSRB case will be discussed more carefully in a subsequent paper). Again, the histogram is in excellent agreement with (28). This implies that, for the lossless case, with a single input transmission line to the cavity, the impedance statistics are not so sensitive to the spacing distributions, as long as they have the same mean value.

The issue of long range correlations in the distribution of eigenvalues doesn't affect statistics of the impedance in the lossless case. In principle, one can also incorporate additional eigenvalue correlation from random matrix theory in the statistics generating the k_n^2 in Eq. (27) (and when losses are considered, this is necessary). We note that the mean and width of the distribution in the random matrix approach are specific to the random matrix problem. In contrast, in our formulation, these quantities are determined by the geometry-specific port coupling to the cavity through the radiation impedance $Z_R(k_n^2)$.

HFSS Simulation Result for the Normalized Impedance

To test our prediction for the distribution function of the normalized impedance, we have computed the impedance for the cavity in Figure 1a for the coupling shown in Figure 1b using the commercially available program HFSS (Ansoft). To create different realizations of the configuration, we placed a small metallic cylinder of radius 0.6 cm and height h at 100 different points inside the cavity. In addition, for each location of the cylinder, we swept the frequency through a 2.0 GHz range (about 100 modes) from 6.75 GHz

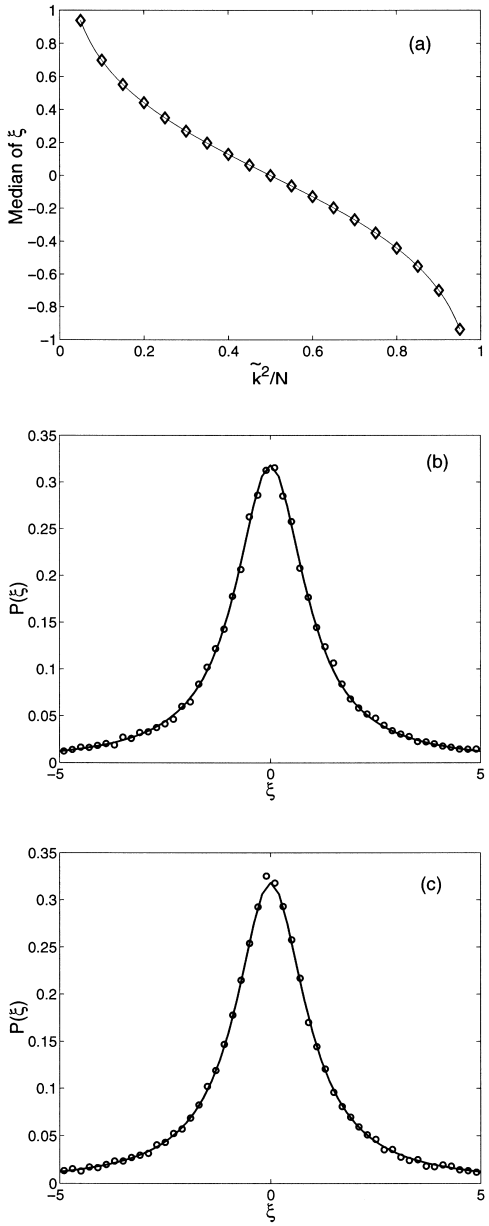

Figure 2. (a) Median of ξ versus $\tilde{k}^2/N$, compared with Eq. (29). (b) Histogram of approximation to $P_\xi(\xi)$ (solid dots) in the TRS case compared with a Lorentzian distribution of unit width. (c) Same as (b) but for the TRSB case.

to 8.75 GHz in 4000 steps of width 5×10^{-4} GHz. We generated 100,000 impedance values. In addition, to obtain the radiation impedance, we also used HFSS to simulate the case with radiation boundary conditions assigned to the sidewalls of the cavity. We find that the average value of the cavity reactance (which we predict to be the radiation reactance) has large systematic fluctuations. This is illustrated in Figure 3, where we plot the median cavity reactance versus frequency. Here the median is taken with respect to the 100 locations of the perturbing disc. Also shown in Figure 3 is the radiation reactance $X_R(\omega) = \mathrm{Im}[Z_R(\omega)]$. As can be seen the radiation reactance varies only slightly over the plotted frequency range, whereas the median cavity reactance has large frequency-dependent fluctuations about this value. On the other hand, we note that over the range 6.75–8.75 GHz, the average radiation reactance is 40.4 Ω and the average of the median cavity reactances is 42.3 Ω. Thus over this frequency band, there is good agreement. The scale of the fluctuations in cavity reactance is on the order of 0.2 GHz, which is much larger than the average spacing between cavity resonances, which is only 0.016 GHz. Thus, these fluctuations are not associated with individual resonances. Rather, the frequency scale of 0.2 GHz suggests that they are multipath interference effects ($L \sim 100$ cm), which survive in the presence of the moveable conducting disc. One possibility is that the fluctuations are the result of scars (Heller, 1984), and this will be investigated in the future. The implication of Figure 3 is that to obtain good agreement with the theory predicting a Lorentzian distribution, it may be necessary to average over a sufficiently large frequency interval.

To test the Lorentzian prediction we normalize the cavity impedance using the radiation impedance as in Eq. (25) and Eq. (26); the normalized impedance values, $\tilde{\xi} = \{\mathrm{Im}[Z(k)] - X_R(k)]\}/R_R(k)$, are computed; and the resulting histogram approximations to $P_{\tilde{\xi}}(\tilde{\xi})$ are obtained. Figure 4a shows the result for the case where we have used data in the frequency range 6.75 GHz to 8.75 GHz (the range plotted in Figure 3). The histogram points are shown as dots, and the theorectical unit width Lorentzian is shown

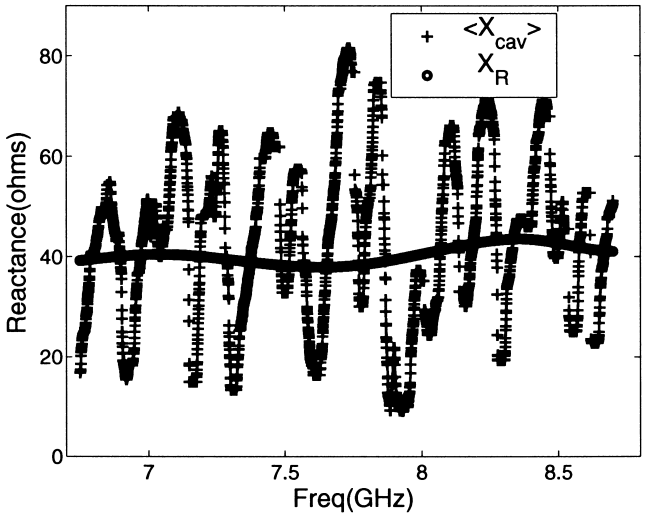

Figure 3. Median cavity reactance averaged over 100 realization versus frequencies ranged from 6.75 GHz to 8.75 GHz, compared with the corresponding radiation reactance $\mathrm{Im}[Z_R(\omega)]$.

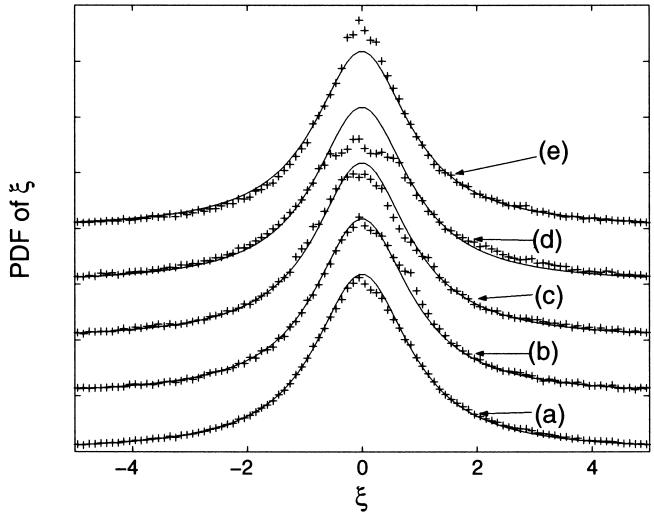

Figure 4. Histogram approximation to $P_\xi(\xi)$ from numerical data calculated using HFSS in different frequency ranges. (a) 6.75–8.75 GHz, (b) 6.75–7.25 GHz, (c) 7.25–7.75 GHz, (d) 7.75–8.25 GHz, (e) 8.25–8.75 GHz.

as a solid curve. Good agreement between the predicted Lorentzian and the data is seen. Figures 4b–e show similar plots obtained for smaller frequency ranges of width 0.5 GHz: (b) 6.75–7.25 GHz, (c) 7.25–7.75 GHz, (d) 7.75–8.25 GHz, (e) 8.25–8.75 GHz. For these narrow frequency ranges, we see that Figures 4b and 4c show good agreement with (28), while, on the other hand, Figures 4d and 4e exhibit some differences. These are possibly associated with the variances in the median cavity reactance shown in Figure 3, as the agreement with the Lorentzian prediction improves when averaging over a large range of frequencies.

Variation in Coupling

In this section, we bolster our arguments connecting the radiation impedance and the normalization of the cavity impedance by showing that the relation is preserved when the details of the coupling port are modified. Let us consider a one-port coupling case in which the actual coupling is equivalent to the cascade of a lossless two-port and a "pre-impedance" Z seen at terminal 2, as illustrated in Figure 5.

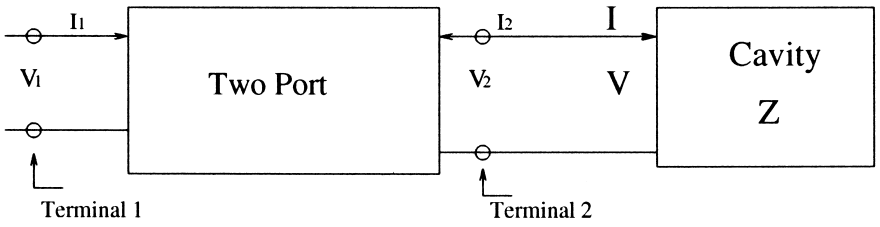

Figure 5. Schematic description of the two-port model.

The impedance Z at terminal 2 then transforms to a new impedance Z' at terminal 1 of the two-port according to

$$Z' = j\hat{X}_{11} + \frac{\hat{X}_{12}\hat{X}_{21}}{j\hat{X}_{22} + Z}, \tag{30}$$

where $j\hat{X}_{ij}$ is now the purely imaginary 2 by 2 impedance matrix of the lossless two-port. We now ask how Z transforms to Z' when (a) Z is the complex impedance Z_R corresponding to the radiation impedance into the cavity (i.e., the cavity boundaries are extended to infinity) and (b) $Z = jX$ is an imaginary impedance corresponding to a lossless cavity, where X has a mean $\bar{X}$ and Lorentzian distributed fluctuation $\tilde{X}$.

First considering case (a), the complex cavity impedance $Z_R = R_R + jX_R$ transforms to a complex impedance $Z'_R = R'_R + jX'_R$, where

$$R'_R = R_R \frac{\hat{X}_{12}\hat{X}_{21}}{R_R^2 + (\hat{X}_{22} + X_R)^2} \tag{31}$$

and

$$X'_R = \hat{X}_{11} - (\hat{X}_{22} + X_R)\frac{\hat{X}_{12}\hat{X}_{21}}{R_R^2 + (\hat{X}_{22} + X_R)^2}. \tag{32}$$

In case (b) we consider the transformation of the random variable X to a new random variable X' according to $X' = \hat{X}_{11} + \hat{X}_{12}\hat{X}_{21}/(\hat{X}_{22} + X)$. One can show that if X is Lorentzian distributed with mean X_R and width R_R then X' will be Lorentzian distributed with mean X'_R and the width R'_R. Thus, the relation between the radiation impedance and the fluctuating cavity impedance is preserved by the lossless two-port. Accordingly, we reassert that this relation holds in general for coupling structures whose properties are not affected by the distant walls of the cavity. A treatment similar to that above has also been given by Brouwer (1995) in the context of scattering with a scattering matrix description of the connection between terminals 1 and 2.

We now summarize the main ideas of this section. The normalized impedance of a lossless chaotic cavity with time-reversal symmetry has a universal distribution which is a Lorentzian. The width of the Lorentzian and the mean value of the impedance can be obtained by measuring the corresponding radiation impedance under the same coupling conditions. The physical interpretation of this correspondence is as follows. In the radiation impedance, the imaginary part is determined by the near field, which is independent of cavity boundaries. On the other hand, the real part of the radiation impedance is related to the far field. In a closed, lossless cavity, the real part of the impedance vanishes. However, waves that are radiated into the cavity are reflected from the boundaries, eventually returning to the port and giving rise to fluctuation in the cavity reactance.

Statistics of Reflection Coefficient in the Lossless Case

In the previous section, we obtained a universal Lorentzian distribution for the chaotic cavity impedance Z, after normalization by the radiation impedance

$$Z = j(X_R + R_R\xi), \tag{33}$$

where ξ is a zero mean, unit width Lorentzian random variable. We now consider the consequences for the reflection coefficient. Suppose we can realize the perfect coupling condition, i.e., $R_R = Z_0$, $X_R = 0$, in which the wave does not "feel" the transition from the cable to the cavity. In this case the cavity reflection coefficient becomes

$$S = \frac{j\xi - 1}{j\xi + 1} = \exp[-j(2\tan^{-1}\xi + \pi)]. \tag{34}$$

A standard Lorentzian distribution for ξ corresponds to a uniform distribution for $\tan^{-1}\xi$ from $[-\pi/2, \pi/2]$ and thus to a reflection coefficient uniformly distributed on the unit circle.

In the general case (i.e., nonperfect coupling), we introduce $\gamma_R = R_R/Z_0$, $\gamma_X = X_R/Z_0$, and express S as

$$S = e^{j\phi} = (Z + Z_0)^{-1}(Z - Z_0) = \frac{j(\gamma_R\xi + \gamma_X) - 1}{j(\gamma_R\xi + \gamma_X) + 1}. \tag{35}$$

We replace the Lorentzian random variable ξ by introducing another random variable ψ via $\xi = \tan(\psi/2)$. Using this substitution, the Lorentzian distribution of ξ translates to a distribution of ψ that is uniform in $[0, 2\pi]$. We then have from Eq. (35)

$$e^{j(\phi - \phi_R)} = \frac{e^{-j\psi'} + |\rho_R|}{1 + |\rho_R|e^{-j\psi'}}, \tag{36}$$

where the "free space reflection coefficient" ρ_R,

$$\rho_R = |\rho_R|e^{j\phi_R} = \frac{\gamma_R + j\gamma_X - 1}{\gamma_R + j\gamma_X + 1}, \tag{37}$$

is the complex reflection coefficient in the case in which the cavity impedance is set equal to the radiation impedance ($\tilde{\xi} = -j$), and $\psi' = \psi + \pi + \phi_R + 2\tan^{-1}[\gamma_X/(\gamma_R + 1)]$ is a shifted version of ψ. Equations for the magnitude and phase of the free space reflection coefficient ρ_R can be obtained from Eq. (37). Specifically,

$$|\rho_R| = \sqrt{\frac{(\gamma_R - 1)^2 + \gamma_X^2}{(\gamma_R + 1)^2 + \gamma_X^2}} \tag{38}$$

and

$$\tan\phi_R = \frac{2\gamma_X}{\gamma_R^2 + \gamma_X^2 - 1}. \tag{39}$$

Equation (36) is essentially a statement of the Poisson kernel relation for a nonperfectly coupled one-port cavity.

To compute the probability distribution function for ϕ, $P_\phi(\phi)$, we note that, since ψ is uniformly distributed on any interval of 2π, we can just as well take ψ', which differs from ψ by a constant shift, to be uniformly distributed. Consequently, we have

$$\begin{aligned} P_\phi(\phi) &= \frac{1}{2\pi}\left|\frac{d\psi'}{d\phi}\right| \\ &= \frac{1}{2\pi}\frac{1 - |\rho_R|^2}{1 + |\rho_R|^2 - 2|\rho_R|\cos(\phi - \phi_R)}. \end{aligned} \tag{40}$$

Thus $P_\phi(\phi)$ is peaked at the angle ϕ_R corresponding to the phase angle of the free space reflection coefficient, with a degree of peaking that depends on $|\rho_R|$, the magnitude of the free space reflection coefficient. "Perfect matching" corresponds to $\gamma_R = 1$, $\gamma_X = 0$, and $|\rho_R| = 0$, in which case $P_\phi(\phi)$ is uniform.

We next consider the case of poor matching for which $|\rho_R| \cong 1$ and $P_\phi(\phi)$ is strongly peaked at ϕ_R. This behavior can be understood in the context of the frequency dependence of the phase for a given realization. It follows from (35) and (27) that the phase ϕ decreases by 2π as k^2 increases by the spacing between eigenvalues. If $|\rho_R| \cong 1$, then for most of the frequencies in this interval, the phase is near ϕ_R. However, for the small range of frequencies near a resonance, the phase will jump by 2π as the resonance is passed. This indicates that the mode of the cavity is poorly coupled to the transmission line. In the case of good matching, $|\rho_R| = 0$, all phases are equally likely, indicating that, as a function of frequency, the rate of increase of phase is roughly constant. This implies that the resonances are broad, and the cavity is well coupled to the transmission line.

In order to describe the different coupling strengths, we consider the parameter g originally introduced by Fyodorov and Sommers (1997):

$$g = \frac{1 + |\langle e^{j\phi} \rangle|^2}{1 - |\langle e^{j\phi} \rangle|^2}. \tag{41}$$

Evaluating $\langle S \rangle$ using Eq. (40),

$$g = \frac{1 + |\rho_R|^2}{1 - |\rho_R|^2}. \tag{42}$$

Thus, g has a minimum value of 1 in the perfectly matched case and is large if the matching is poor, $|\rho_R| \sim 1$. An analogous quantity is the voltage standing wave ratio on the transmission line when the cavity impedance is set equal to the radiation impedance,

$$\text{VSWR} = \frac{1 + |\rho_R|}{1 - |\rho_R|} = g + \sqrt{g^2 - 1}. \tag{43}$$

To test Eq. (40), we compared its predictions for the phase distribution with direct numerical calculations obtained using HFSS (High Frequency Structure Simulator) for the case of the cavity and coupling detail as specified in Figure 4. As compared to what was done for Figure 4, we have narrowed the frequency range to 0.1 GHz bands for each realization in 1000 10^{-4} GHz steps centered at 7 GHz, 7.5 GHz, 8 GHz, and 8.5 GHz. Instead of calculating the radiation impedance for every frequency, we use the value of Z_R at the middle frequency of the interval in calculating the values of γ_R and γ_X. We present theoretical phase density distribution functions together with numerical histogram results in Figure 6. The agreement between the theory, Eq. (40), and the numerical results is surprisingly good, especially considering the rather small (0.1 GHz) frequency range used.

Effect of Distributed Losses

We now consider the effect of distributed losses in the cavity. By distributed losses, we mean losses that affect all modes in a frequency band equally (or at least approximately so). For example, wall losses and losses from a lossy dielectric that fills the cavity

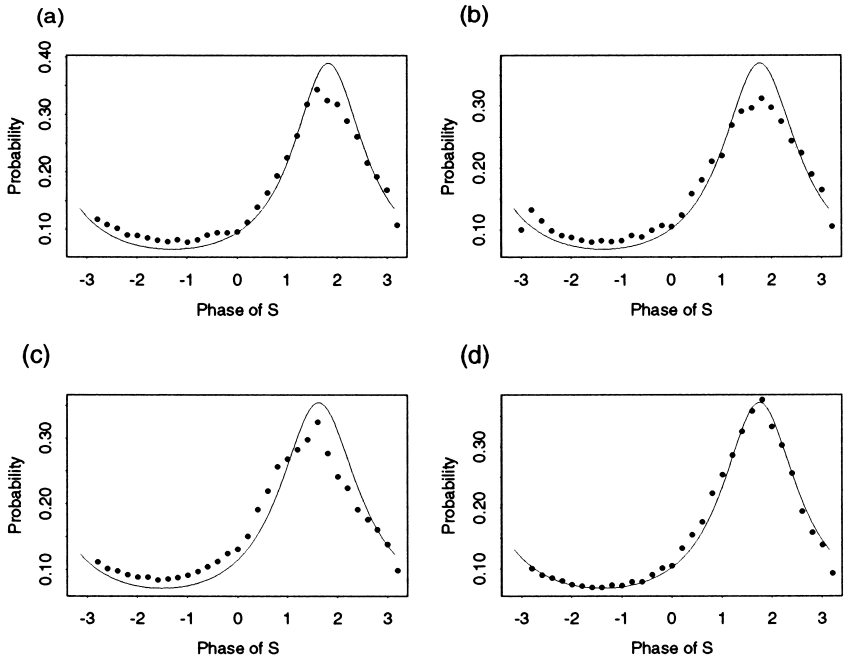

Figure 6. Histogram of the reflection phase distribution for an HFSS calculation for the cavity in Figure 1 with center frequencies located at (a) 7 GHz, (b) 7.5 GHz, (c) 8 GHz, (d) 8.5 GHz, and with sweeping span equal to 0.1 GHz. Numerical data are compared with Eq. (40) using parameters determined by Z_R at the corresponding center frequencies.

are considered distributed. (For the case of losses due to conducting walls, the losses are approximately proportional to the surface resistivity, $\sim \sqrt{f}$, and vary little in a frequency range $\Delta f \ll f$. In addition, there will also be variation of wall losses from mode to mode due to different eigenmode structural details. These modal fluctuations, however, are small when the modes are chaotic and the wavelength is short.) We use the random coupling model to construct a complex cavity impedance accounting for distributed losses in a manner analogous to the lossless case, Eq. (18),

$$Z = -\frac{j}{\pi} \sum_n \Delta \frac{R_R(k_n) w_n^2}{k^2(1 - j\sigma) - k_n^2}, \tag{44}$$

where σ represents the effect of losses. In particular, for loss due to wall absorption in a two-dimensional cavity, the value of σ is equal to the ratio of the skin depth of the conductor to the height of the cavity; if the cavity contains a lossy dielectric, σ is the loss tangent of the dielectric. The cavity quality factor is related to σ by $\sigma = Q^{-1}$. This follows by noting that the real part of Z will have a Lorentzian dependence on frequency ($\omega = kc$) peaking at $\omega = k_n c$ with a full width at half maximum of $\omega\sigma$.

The impedance Z will have a real part and an imaginary part. We expect that, if $k^2\sigma \ll \Delta$, corresponding to small losses, then the real part will be zero and the imaginary part will have an approximately Lorentzian distribution. As losses are increased such that

$k^2\sigma \sim \Delta$ (the imaginary part of the denominators in (44) is of the order of eigenvalue spacing), the distributions of the real and imaginary part will change, reflecting that extremely large values of $|Z|$ are no longer likely. In the high loss limit, $k^2\sigma \gg \Delta$, many terms in the sum contribute to the value of Z. In this case, we expect that Z will approach the radiation impedance with small (Gaussian) fluctuations.

In the appendix we evaluate the mean and variance of the real and imaginary part of the complex impedance (44) $Z = R + jX$. There it is shown that the mean is the radiation impedance $Z_R = R_R + jX_R$, and the variances of the real and imaginary parts are equal: $Var[R] = Var[X]$. In general, the distribution of R and X depends on the correlations between eigenvalues of k_n^2. However, in the low damping limit, the correlations are unimportant and we obtain

$$Var[R] = \frac{3R_R^2}{2\pi}\frac{\Delta}{k^2\sigma} \tag{45}$$

for both the TRS and the TRSB cases. In the high damping limit $k^2\sigma \gg \Delta$, correlations are important and we obtain

$$\begin{aligned} Var[R] &= \frac{R_R^2}{\pi}\frac{\Delta}{k^2\sigma} \qquad \text{for the TRS case,} \\ Var[R] &= \frac{R_R^2}{2\pi}\frac{\Delta}{k^2\sigma} \qquad \text{for the TRSB case.} \end{aligned} \tag{46}$$

This is to be contrasted with the result one would obtain if correlations in the eigenvalue spacing were neglected; i.e., if the k_n were assumed to be generated by adding independent spacings generated from the distributions (16) and (17). In that case, using the method in the appendix, one obtains

$$\begin{aligned} Var[R] &= \frac{R_R^2}{\pi}\frac{\Delta}{k^2\sigma}\left(\frac{1}{2} + \frac{2}{\pi}\right) \qquad \text{for the TRS case,} \\ Var[R] &= \frac{R_R^2}{\pi}\frac{\Delta}{k^2\sigma}\left(\frac{3\pi}{16}\right) \qquad \text{for the TRSB case.} \end{aligned} \tag{47}$$

These results are larger than those in Eq. (46) by 13.7% in the TRS case and 17.8% in the TRSB case, thus illustrating the necessity of generating the k_n^2 using random matrix theory if accurate results are desired in the lossy case $k^2\sigma > \Delta$.

In a recent experimental paper (Warne et al., 2003), the impedance statistics of a lossy TRS one-port microwave cavity were also considered. Their result is the same as (44). One difference is that they generate the realizations of k_n^2 solely by use of Eq. (16) with the assumption that the eigenvalue spacings are random independent variables.

We now investigate a model, normalized impedance, applicable in the one-port case with loss, which is the generalization of Eq. (27):

$$\zeta(\sigma) = -\frac{j}{\pi}\sum_{n=1}^{N}\frac{w_n^2}{\tilde{k}^2(1 - j\sigma) - \tilde{k}_n^2}. \tag{48}$$

The normalized impedance ζ will have a real part $\rho > 0$ and an imaginary part ξ, $\zeta = \rho + j\xi$. We expect that if $\tilde{k}^2\sigma \ll 1$, corresponding to small loss, then $\rho \cong 0$, and ξ will have an approximately Lorentzian distribution.

In analogy to Eq. (26) we write for the cavity impedance

$$Z = jX_R + R_R\zeta, \tag{49}$$

and we use (48) to generate probability distribution functions for the real and imaginary part of $\zeta = \rho + j\xi$. We first generate N values of w_n as independent Gaussian random variables of unit width (for this purpose we use a suitable random number generator). We next generate N values of the normalized eigenvalues $\tilde{k}_n^2$. To do this we have utilized two methods: (i) an approximate method based on Eq. (16) (for the TRS case) or Eq. (17) (for the TRSB case), and (ii) a method based on random matrix theory. We pick the value of k^2 relative to the spectrum k_n^2 such that the median of ξ is zero.

For method (i) we independently generate N values of s_n using the distribution (16) or (17). We then obtain $\tilde{k}_n^2$ as $\tilde{k}_n^2 = \sum_{n'=1}^{n} s_{n'}$. The main assumption of this method is that the spacings s_n can be usefully approximated as uncorrelated. On the other hand, it is known from random matrix theory that the spacings are correlated over long distance (in n), and the thus the assumption of method (i) is questionable (compare (46) and (47)). This motivates our implementation of method (ii). (See also Kogan, Mello, & Liqun (2000).)

To implement method (ii) we generate an $M \times M$ random matrix with M large ($M = 1000$) drawn from the appropriate ensemble (GOE or GUE), again using a random number generator. The width of the diagonal elements is taken to be unity. We then numerically determine the eigenvalues. The average spacing between eigenvalues of random matrices is not uniform. Rather, in the limit of large M, the eigenvalues λ are distributed in the range $-\sqrt{2M} < \lambda < \sqrt{2M}$, and the average spacing for eigenvalues near an eigenvalue λ is given by

$$\Delta(\lambda) = \pi/\sqrt{2M - \lambda^2} \tag{50}$$

in both the TRS and TRSB cases. In order to generate a sequence of eigenvalues with approximately uniform spacing we select out the middle 200 levels. We then normalize the eigenvalues by multiplying $1/\Delta(0)$ to create a sequence of $\tilde{k}_n^2$ values with average spacing of unity.

Histogram approximations to the GOE probability distributions of $\mathrm{Re}[\zeta]$ and $\mathrm{Im}[\zeta]$ obtained by use of (48) and method (ii) are shown in Figures 7a and 7b. These were obtained using 30,000 random GOE matrix realizations of 1000 by 1000 matrices and selecting the middle 200 eigenvalues of each realization. The resulting graphs are shown for a range of damping values, $\tilde{k}^2\sigma = 0.01$, 0.1, 0.5, 1, 5, and 10. As seen in Figure 7a, when $\tilde{k}^2\sigma$ is increased, the distribution of ξ values becomes "squeezed." Namely, the Lorentzian tail disappears and the fluctuations in ξ decrease. Eventually, when σ enters the regime, $1 \ll \tilde{k}^2\sigma \ll N$, the probability distribution function of $\xi(\sigma)$ approaches a narrow Gaussian distribution centered at $\xi = 0$ (recall that $\bar{\xi} = 0$). As shown in Figure 7b, as σ increases from zero, the distribution of the real part of $\zeta(\sigma)$ which, for $\sigma = 0$, is a delta function at zero, expands and shifts toward 1, becoming peaked around 1. In the very high damping case, both the real and the imagnary parts of ζ, ρ, and ξ will be Gaussian distributed with the mean value equal to 1 and 0, respectively, and the same variance inversely proportional to the loss (as shown in the appendix). As a consequence,

the reflection coefficient $|S|^2$ in the high damping limit is exponentially distributed. This result is consistent with the theoretical discussion given by Kogan, Mello, and Liqun (2000).

In general, the complex impedance distribution is not described using simple distributions such as Gaussian or Lorenzian. The distribution of the real part of the impedance has been studied in connection with the theory of mesoscopic systems and known as the "local density of states" (LDOS). Through the supersymmetry approach, Efetov obtained the probability density function for the LDOS in systems without time reversal symmetry (Efetov & Prigodin, 1993). For chaotic systems with time reversal symmetry, the corresponding exact formula was derived in a form of multiple integral (Taniguchi & Prigodin, 1996). However, the difficulty in carrying out the fivefold integral makes it hard to interpret the formulus in Taniguchi and Prigodin (1996). Very recently, Fyodorov and Savin (2004) have proposed an interpolation formulas for the impedance distributions at arbitary values of damping parameter. The suggested formulas satisfy all the asymptotic behaviors in the physically interesting limiting cases, e.g., weak damping or very string damping cases. Furthermore, these formulas seem to agree pretty well with the results of the numerical simulations, though the agreement in the intermediate damping case is not as good as in the limiting cases. In our paper, we still use the histograms generated from the Monte-Carlo simulations as a comparison to the HFSS data; however, we believe the formula presented by Fyodorov and Savin would be very helpful for most practical purposes of comparison.

We noted that the variance of the real and imaginary parts of the complex impedance are equal. There is a more fundamental connection between these that is revealed by considering the reflection coefficient in the perfectly matched case,

$$\alpha e^{j\phi} = (\zeta - 1)/(\zeta + 1), \tag{51}$$

where α and ϕ are random variables giving the magnitude and phase of the reflection coefficient. It can be argued (Kogan, Mello, & Liqun, 2000) that ϕ and α are independent and that ϕ is uniformly distributed in $[0, 2\pi]$. The magnitude α is distributed on the interval [0, 1] with a density that depends on losses. A plot of the probability distribution for α taken from the data in Figures 7a and 7b is shown in Figure 8 for the damping values 0.1, 0.5, 1, and 5.

We can express the actual complex reflection coefficient ρ in terms of the normalized reflection coefficient by first finding the normalized impedance from (51), $\zeta = (1 + \alpha e^{j\phi})/(1 - \alpha e^{j\phi})$, calculating the cavity impedance from (49), and expressing the result in terms of the radiation reflection coefficient (37). The result is

$$\rho = \frac{\rho_R + \alpha e^{j(\phi+\Delta\phi)}}{1 + \alpha e^{j(\phi+\Delta\phi)}\rho_R^*}, \tag{52}$$

where $\tan(\Delta\phi/2) = -X_R/(R_R + Z_0)$ depends on system-specific parameters. Since the angle ϕ is uniformly distributed, it can be shifted by $\Delta\phi$, thus eliminating $\Delta\phi$ from the expression. Equation (52) is then a restatement of the Poisson kernel in the single port case.

The independence of α and ϕ in Eq. (51) also guarantees the invariance of the distribution of cavity impedances when a lossless two-port is added as discussed previously. In particular, the normalized cavity impedance ζ before the addition of the

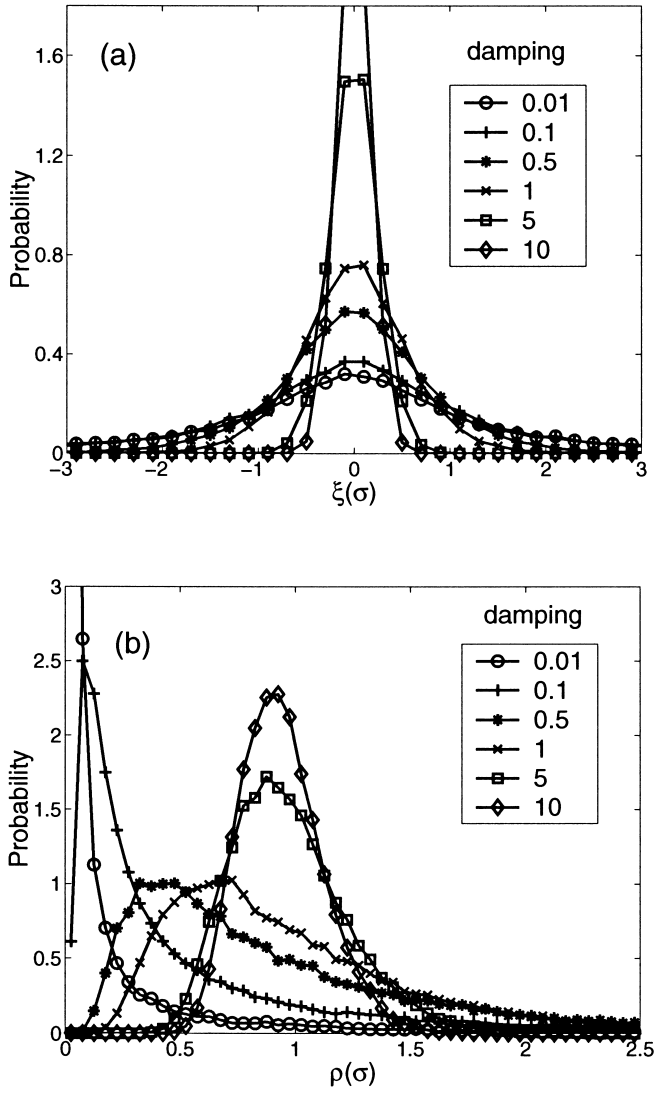

Figure 7. (a) Histogram of the imaginary part of $\zeta(\sigma)$ with different values of the damping obtained with method (ii); (b) histogram of the real part of $\zeta(\sigma)$ with different dampings obtained with method (ii)

two-port is given by

$$\zeta = \frac{Z - jX_R}{R_R} = \frac{1 + \alpha e^{j\phi}}{1 - \alpha e^{j\phi}}. \tag{53}$$

With the addition of the lossless two-port as shown in Figure 5, impedances are transformed to Z', X'_R, and R'_R such that

$$\zeta = \frac{Z' - jX'_R}{R'_R} = \frac{1 + \alpha e^{j(\phi - \phi_c)}}{1 - \alpha e^{j(\phi - \phi_c)}}, \tag{54}$$

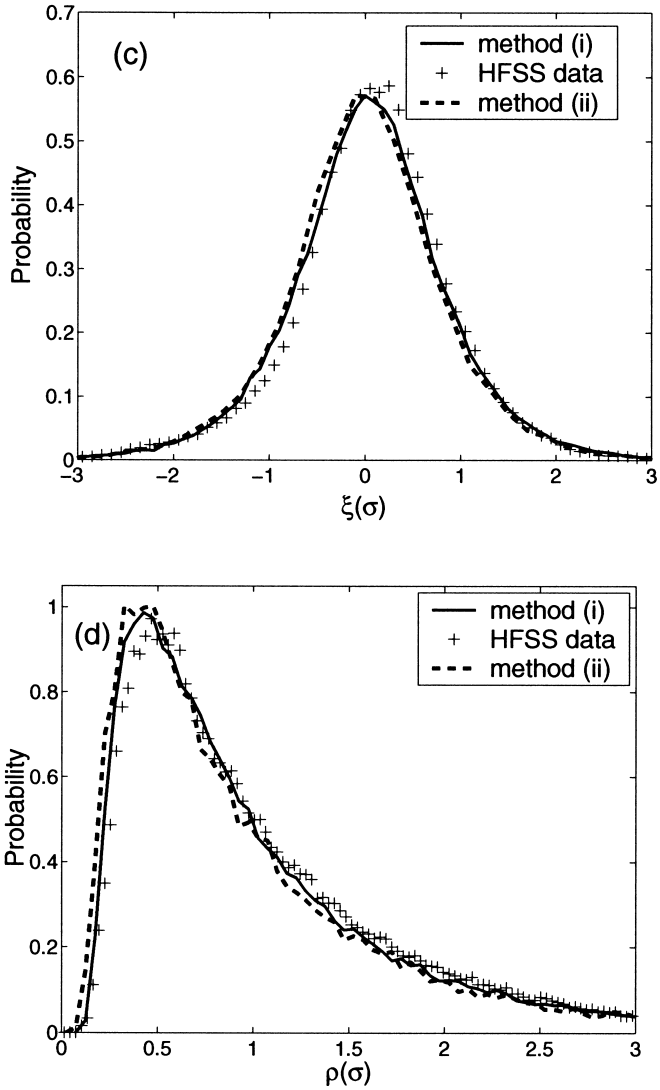

Figure 7. (c) and (d) are histograms of the reactance and resistance from HFSS calculation with a lossy top and bottom plate, compared with histograms from Eq. (48) computed as in (a) and (b) (dashed line) and by method (i) (solid line).

where $\phi_c = (2\beta + \pi)$ depends only on the properties of the two port and the cavity coupling port, and the angle β satisfies

$$\cos\beta = \frac{R_R}{\sqrt{R_R^2 + (X_{11} + X_R)^2}}, \qquad \sin\beta = \frac{(X_{11} + X_R)}{\sqrt{R_R^2 + (X_{11} + X_R)^2}}. \tag{55}$$

Since ϕ is uniformly distributed, so is the difference $\phi - \phi_c$. Consequently, the normalized random variables ζ and ζ' have identical statistical properties.

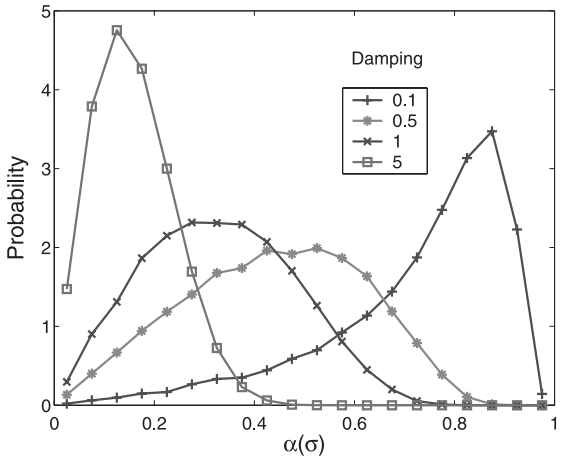

Figure 8. Histogram of the magnitude of reflection coefficient in the Eq. (51), $\alpha(\sigma)$, with different values of the damping.

A by-product of (53) is that we can easily prove that its real part $\rho = (1-\alpha^2)/(1+\alpha^2-2\alpha\cos\phi)$ and its imaginary part $\xi = (2\alpha\sin\phi)/(1+\alpha^2-2\alpha\cos\phi)$ have the same variance and zero correlation. Since α and ϕ are independent, we can carry out the integration over the uniformly distributed ϕ and obtain

$$Var[\rho] = Var[\xi] = \left\langle \frac{1+\alpha^2}{1-\alpha^2} \right\rangle_\alpha - 1, \qquad Cov[\rho, \xi] = 0, \tag{56}$$

where $\langle .. \rangle_\alpha$ denotes the average over α. This property has been tested in microwave cavity experiments with excellent agreement (Hemmady et al., 2004). For the high damping case, $\rho - 1$ and ξ will become two independent Gaussian variables with zero mean and small but same variances. This yields an exponential distribution for the α^2, which is consistent with the result obtained by Kogan, Mello, and Liqun (2000) based on the "maximum information entropy" principle. For the weakly absorpting case, Beenakker and Brouwer (2001) studied the distribution of α^2 in the TRSB case through the time-delay matrix and obtained a generalized Laguerre ensemble. However, for a TRS system with arbitary loss, there is no simple formula for the distribution of reflection coefficients.

Using HFSS, we simulate the lossy case by specifying the material on the top and bottom plates to be an imperfect conductor with a bulk resitivity of 70 mΩ·cm. In this case we can calculate a value of $\sigma = \delta/h = 0.002$, where δ is the skin depth and h the cavity height. The corresponding parameter $\tilde{k}^2\sigma$ is 0.5 at 7.75 GHz. Histogram results for the normalized reactance (ξ) and resistance (ρ) fluctuations of $\zeta_{hfss} = R_R^{-1}(Z_{cav} - jX_R) = \rho + j\xi$ are plotted in Figures 7c and 7d together with the histograms generated from Eq. (48) and using spectra from the random matrices. As can be seen, the histograms from the HFSS simulations match those of the model.

Summary

We have applied the concepts of wave chaos to the problem of characterizing the statistics of the impedance and scattering coefficient for irregular electromagnetic cavities with one port in the small wavelength regime. The coupling of energy in and out of the port in such cavities depends on both the geometry of the port and the geometry of the cavity.

We found that these effects can approximately be separated. The geometry of the port is characterized by its radiation impedance which has both a real and an imaginary part. This impedance describes the port in the case in which the distant walls of the cavity are treated as perfect absorbers (or else are removed to infinity). The effects of the geometry of the cavity can be treated in a statistical way using Random Marix Theory. The separation of the system-specific aspects of the coupling and the universal aspects has previously been described using the Poisson kernel (Mello, Peveyra, & Seligman, 1985). The relation of our approach to the Poisson kernel may be understood by comparing the equivalent relations (49) and (52). To extract a universal quantity (ζ) from a set of impedance values (Z) one must subtract the radiation reactance and normalize to the radiation resistance. To extract a universal quantity ($\alpha e^{j\phi}$) from a set of reflection values (ρ) we must solve the bilinear relation (52) for the magnitude α and phase ϕ of the normalized reflection coefficient. The normalized impedance and scattering amplitude are related by $\alpha e^{j\phi} = (\zeta - 1)/(\zeta + 1)$. If the radiation reflection coefficient ρ_R is known, then (52) may be solved directly for normalized reflection coefficient,

$$\alpha e^{j\phi} = e^{-j\Delta\phi} \frac{\rho - \rho_R}{1 - \rho\rho_R^*}. \tag{57}$$

The radiation reflection coefficient can be determined directly by measurement (Hemmady et al., 2004) or by ensemble averaging. According to Mello, Peveyra, and Seligman (1985) the average of ρ is equal to ρ_R. This can be verified directly from (52) by averaging over the uniformly distributed phase ϕ. Regardless of the value of α, one finds

$$\int \frac{d\phi}{2\pi} \rho = \rho_R. \tag{58}$$

Thus if enough appropriate, statistically independent realizations are available to compute the average of ρ, (58) can be used to find the universal reflection amplitude.

Consistent with previous results (Mello, Peveyra, & Seligman, 1985) our model predicts that in the lossless case the impedance is Lorentzian distributed with a mean equal to the radiation reactance and a width equal to the radiation resistance. The Lorentzian prediction is tested by direct numerical solution of Maxwell's equation for the cavity of Figure 1. The predictions are verified if an additional averaging over frequency is introduced. Effects of distributed loss and variation of coupling are also investigated and we have generated PDFs for the real and imaginary parts of the normalized impedance. In addition, we have calculated the mean and variance for these distributions and determined the effect of correlations in the eigenfrequencies on the variances. The values of the variance depend on the degree of loss in the cavity and can be used to quantify it. Finally, we have compared the predicted distributions of the normalized impedance with those obtained from a direct numerical simulation.

Appendix: Variance of Cavity Reactance and Resistance in the Lossy Case

From Eq. (44), we obtain the expression for the complex impedance in the single port case,

$$\begin{aligned} Z(\sigma) &= \frac{1}{\pi} \sum_{1}^{N} \left[\frac{\Delta(k_n^2) R_R(k_n^2) w_n^2 [k_d^2 + j(k_n^2 - k^2)]}{(k^2 - k_n^2)^2 + (k_d^2)^2} \right] \\ &= R(\sigma) + jX(\sigma), \end{aligned} \tag{A.1}$$

where Δ is the mean spacing $\langle k_n^2 - k_{n-1}^2 \rangle$, $X(\sigma)$ and $R(\sigma)$ are cavity reactance and resistance in the lossy case, and $k_d^2 = k^2\sigma$. In this appendix, we are going to evaluate the mean and variance of $X(\sigma)$ and $R(\sigma)$ as well as their covariance.

We first investigate the mean of $R(\sigma)$. We express the mean in terms of probability distribution function for the eigenvalues k_n^2:

$$E[R(\sigma)] = \frac{1}{\pi} \int \cdots \int dk_1^2 \ldots dk_N^2 P_J(k_1^2, \ldots, k_N^2) \sum_{n'=1}^{N} \frac{R_R \Delta \langle w_{n'}^2 \rangle k_d^2}{(k^2 - k_{n'}^2)^2 + k_d^4}, \tag{A.2}$$

where P_J is the joint distribution of eigenlevels $(k_1^2, \ldots, k_N^2)$ assuming they are unordered. Since the levels are not ordered, in each term of the sum, we can integrate over all $k_n^2 \neq k_{n'}^2$ and obtain N identical terms. Thus,

$$E[R(\sigma)] = \frac{N}{\pi} \int dk_{n'}^2 P_1(k_{n'}^2) R_R \Delta \langle w^2 \rangle \frac{k_d^2}{(k^2 - k_{n'}^2)^2 + k_d^4}, \tag{A.3}$$

where $P_1(k_{n'}^2)$ is the distribution for a single level. Here we have introduced an integer N representing the total number of levels. We will take the limit of $N \to \infty$. The single-level probability distribution then satisfies by definition

$$P_1(k_{n'}^2) = \frac{1}{N \Delta(k_{n'}^2)}. \tag{A.4}$$

We next assume that the radiation resistance $R_R(k_{n'}^2)$ is relatively constant over the interval of $k_{n'}^2$ values satisfying $|k^2 - k_{n'}^2| < k_d^2$ and we will move it outside the integral, replacing it by $R_R(k^2)$. Assuming that k_d^2 is not too large ($k_d^2 \ll k^2$), we can take the end points at the integral to plus and minus infinity and evaluate Eq. (A.3) as

$$E[R] = \frac{R_R}{\pi} \int_{-\infty}^{\infty} dx \frac{1}{x^2 + 1} = R_R(k^2), \tag{A.5}$$

where $x = (k_{n'}^2 - k^2)/k_d^2$. Thus the expected value of the real part of cavity impedance is the radiation resistance independent of the amount of damping. This is somewhat surprising since we have previously asserted that in the lossless case, the cavity resistance is zero. The constancy of the expected resistance results from the resonant nature of the cavity impedance. When losses are small, $k^2\sigma = k_d^2 \ll 1$, for almost all frequencies the resistance is small. However, for the small set of frequencies near a resonance, the resistance is large. This is evident in the histograms of Figure 7b. The result is that a small chance of a large resistance and a large chance of a small resistance combine to give an expected value resistance which is constant.

In order to obtain the variance of $R(\sigma)$, we calculate the second moment of $R(\sigma)$,

$$\begin{aligned} E[R(\sigma)^2] = \left(\frac{1}{\pi}\right)^2 \int \cdots \int \; dk_1^2 \ldots dk_N^2 P_J(k_1^2, \ldots, k_N^2) \sum_{n', m'=1}^{N} \\ \cdot \frac{\Delta^2 R_R(k_{n'}^2) R_R(k_{m'}^2) \langle w_{m'}^2 w_{n'}^2 \rangle k_d^4}{((k^2 - k_{m'}^2)^2 + k_d^4)((k^2 - k_{n'}^2)^2 + k_d^4)} \\ \equiv I_1 + I_2. \end{aligned} \tag{A.6}$$

Following the arguments advanced to calculate $E[R(\sigma)]$, we note that there will be N terms in the double sum for which $k_{n'}^2 = k_{m'}^2$, giving

$$I_1 = \frac{N}{\pi^2} \int dk_{n'}^2 P_1(k_{n'}^2) \frac{\Delta^2 R^2(k_{n'}^2) \langle w_{n'}^4 \rangle k_d^4}{[(k^2 - k_{n'}^2)^2 + k_d^4]^2}, \tag{A.7}$$

and $N(N-1)$ terms for which $k_{m'}^2 \neq k_{n'}^2$, giving

$$I_2 = N(N-1) \iint dk_{n'}^2 dk_{m'}^2 \frac{P_2(k_{n'}^2, k_{m'}^2) \Delta(k_{n'}^2) \Delta(k_{m'}^2 R_R(k_{n'}^2) R_R(k_{m'}^2) \langle w_{n'}^2 \rangle \langle w_{m'}^2 \rangle k_d^4}{[(k^2 - k_{n'}^2)^2 + k_d^4][(k^2 - k_{m'}^2)^2 + k_d^4]}. \tag{A.8}$$

For the first integral we use (A.4) for the single-level distribution function, and making the same approximation as before, we obtain

$$I_1 = R_R^2(k^2) \frac{\langle w^4 \rangle \Delta(k^2)}{2\pi k_d^2}. \tag{A.9}$$

For the second integral we need to introduce the two-level distribution function. For the spectra that we consider, the two-level distribution has the form

$$P_2(k_{n'}^2, k_{m'}^2) = \left(\frac{1}{N\Delta} \right)^2 [1 - g(|k_{n'}^2 - k_{m'}^2|)]. \tag{A.10}$$

Here the function g describes the correlations between two energy levels. For uncorrelated levels giving a Poisson distribution of spacings we have $g = 0$. In the presence of level repulsion we expect $g(0) = 1$ with $(1 - g) \propto |k_{n'}^2 - k_{m'}^2|^\beta$ for small spacing, and $\beta = 1$ for TRS and $\beta = 2$ for TRSB systems. As $|k_{n'}^2 - k_{m'}^2| \to \infty$, $g \to 0$ indicates loss of correlation for two widely separated levels. The function g will be different for spectra produced by random matrices and spectra generated from sequences of independent spacings. Expressions of g for the spectra of random matrices can be found in the book by Mehta (1991; see Chaps. 5 & 6). We will derive the expression for g for spectra generated by sequences of independent spacings later in this appendix.

Based on expression (A.10) and the usual assumptions on the slow variations of R_R and Δ with eigenvalue $k_{n'}^2$ we obtain

$$I_2 = (E[R])^2 - I_g, \tag{A.11}$$

where the first term comes from the 1 in A.10 and the second term comes from the correlation function g:

$$I_g = \frac{R_R(k^2) \langle w^2 \rangle^2}{\pi} \int_{-\infty}^{\infty} \frac{d\tilde{k}^2}{k_d^2} \frac{2}{4 + (\tilde{k}^2/k_d^2)^2} g(|\tilde{k}^2|). \tag{A.12}$$

The variance of R is thus given by

$$\begin{aligned} Var[R] &= E[R]^2 - E[R^2] \\ &= \frac{R_R^2}{\pi} \frac{\Delta}{k_d^2} \left[\frac{\langle w^4 \rangle}{2} - \langle w^2 \rangle^2 \int_{-\infty}^{\infty} \frac{d\tilde{k}^2}{\Delta} \frac{2g(|\tilde{k}^2|)}{4 + (\tilde{k}^2/k_d^2)^2} \right]. \end{aligned} \tag{A.13}$$

Note that since w is a Gaussian random variable with zero mean and unit variance, $\langle w^2\rangle = 1$ and $\langle w^4\rangle = 3$.

Equation (A.13) shows that the variances of R depend on k_d^2/Δ, the ratio of the damping width to the mean spacing of eigenvalues. In the low damping case, $k_d^2/\Delta \ll 1$, the integrand in (A.13) is dominated by the values of $|\tilde{k}^2| < \Delta$ and we replace g by its value $g(0)$. Doing the integral we find

$$Var[R] = R_R^2 \left[\frac{\Delta}{k_d^2} \frac{\langle w^4\rangle}{2\pi} - g(0)\langle w^2\rangle^2 \right]. \tag{A.14}$$

Since the damping is small, the first term dominates and the variance is independent of the eigenvalue correlation function. This is consistent with our previous findings that the eigenvalue statistics did not affect the distribution of reactance values.

In the high damping limit, $k_d^2 > \Delta$, the integral in (A.13) is dominated by $\tilde{k}^2$ values of order Δ, and we have

$$Var[R] = \frac{R_R^2}{\pi} \frac{\Delta}{k_d^2} \left[\frac{3}{2} - \int_0^\infty \frac{d\tilde{k}^2}{\Delta} g(|\tilde{k}^2|) \right]. \tag{A.15}$$

The variance decreases as damping increases with a coefficient that depends on the correlation function. Physically the correlations are important because in the high damping case a relatively large number of terms in the sum (A.1) contribute to the impedance and the sum is sensitive to correlations in these terms.

The integral of the correlation function can be evaluated for different spectra. For spectra generated from random matrices, we have (Mehta, 1991)

$$g(s) = f(s)^2 - \frac{\partial f}{\partial s} \left[\left(\int_0^s ds' f(s') \right) - \frac{1}{2} sgn(s) \right] \tag{A.16}$$

for TRS matrices and

$$g(s) = f(s)^2 \tag{A.17}$$

for TRSB matrices, where $f(s) = \sin(\pi s)/(\pi s)$. In both cases, we find

$$\int_0^\infty ds g(s) = \frac{1}{2}. \tag{A.18}$$

However, to consider the TRSB case we need to repeat the calculation including complex values of the Gaussian variable w. The result is

$$Var[R(\sigma)] = \frac{R_R^2}{\pi} \frac{\Delta}{k_d^2} \left[1 - \int_0^\infty \frac{d\tilde{k}^2}{\Delta} g(|\tilde{k}^2|) \right]. \tag{A.19}$$

For spectra generated by sequences of independent spacing distributions we will show

$$\int_0^\infty \frac{d\tilde{k}^2}{\Delta} g(|\tilde{k}^2|) = 1 - \frac{1}{2}\langle s^2\rangle, \tag{A.20}$$

where $\langle s^2 \rangle$ is the expected value for the normalized nearest neighbor spacing squared. Using (16) and (17), this gives

$$\int_0^\infty \frac{d\tilde{k}^2}{\Delta} g(|\tilde{k}^2|) = \begin{cases} 1 - \dfrac{2}{\pi} & \text{for TRS,} \\ 1 - \dfrac{3\pi}{16} & \text{for TRSB.} \end{cases} \tag{A.21}$$

Note also that (A.20) gives the required value of zero for Poisson spacing distributions, where $\langle s^2 \rangle = 2$.

We can evaluate the expected value of the reactance and its variance, as well as the covariance of reactance and resistance, using the same approach. We find that the expected value of reactance is given by the radiation reactance,

$$E[X] = X_R(k^2). \tag{A.22}$$

The variance of the reactance is equal to that of the resistance (A.13); the covariance between them is zero.

We now derive the g-integral (A.20) for spectra generated from independent spacings. We introduce a conditional distribution $P_m(s)$ that is the probability density that the m^{th} eigenvalue is in the range $[s,\ s + ds]$ given that eigenvalue $m = 0$, is at zero. For convenience, here s is the normalized spacing with unit mean. When $m = 1$, $P_1(s)$ is the spacing distribution $p(s)$. Thus, $1 - g(s)$ stands for the probability that there exists an eigenlevel at $[s, s + ds]$ given one level located at 0. This equality can be expressed as the summation of $P_m(s)$,

$$1 - g(s) = \sum_{m=1}^{\infty} P_m(s). \tag{A.23}$$

$P_m(s)$ can be evaluated assuming the spacings are independent,

$$1 - g(s) = \sum_{m=1}^{\infty} \left[\int \prod_{i=1}^{m} ds_i \, P_1(s_i) \delta \left(s - \sum_{i=1}^{m} s_i \right) \right]. \tag{A.24}$$

We Laplace transforme both sides of Eq. (A.24), and obtain

$$\frac{1}{\tau} - \int_0^\infty ds e^{-\tau s} g(s) = \sum_{m=1}^{\infty} [\bar{P}_1(\tau)]^m = \frac{\bar{P}_1(\tau)}{1 - \bar{P}_1(\tau)}. \tag{A.25}$$

To evaluate $\int_0^\infty ds g(s)$, we take the limit of $\tau \to 0$. The transform $\bar{P}_1(\tau)$ can be expressed in terms of the moments of $P_1(s)$,

$$\begin{aligned} \bar{P}_1(\tau) &= \int_0^\infty e^{-s\tau} P_1(s) ds \\ &\sim \int_0^\infty \left(1 - s\tau + \frac{s^2\tau^2}{2} \right) P_1(s) ds \\ &= 1 - \tau \langle s \rangle + \frac{\tau^2}{2} \langle s^2 \rangle. \end{aligned} \tag{A.26}$$

Thus, we can evaluate the integration of $g(s)$ to be

$$\begin{aligned}\int_0^\infty dsg(s) &= \lim_{\tau\to 0}\int_0^\infty dse^{-\tau s}g(s)\\ &= \lim_{\tau\to 0}\left[\frac{1}{\tau}-\frac{\bar{P}_1(\tau)}{1-\bar{P}_1(\tau)}\right]\\ &= 1-\frac{1}{2}\langle s^2\rangle,\end{aligned} \tag{A.27}$$

which is Eq. (A.20).

References

Ansoft. http://www.ansoft.com/products/hf/hfss/.

Barthélemy, J., O. Legrand, & F. Mortessagne. 2004. Preprint, cond-mat/0401638, submitted to *Phys. Rev. E*; see also J. Barthélemy, O. Legrand, & F. Mortessgne. Preprint (2004), cond-mat/0402029, submitted to *Phys. Rev. Lett.*

Beenakker, C. W. J., & P. W. Brouwer. 2001. *Physica E* 9:463.

Berry, M. V. 1983. *Chaotic behavior of deterministic systems. Les Houches summer school 1981*. Amsterdam: North-Holland.

Brouwer, P. W. 1995. *Phys. Rev. B* 51:16878.

Doron, E., & U. Smilansky. 1990. *Phys. Rev. Lett.* 65:3072.

Efetov, K. B., & V. N. Prigodin. 1993. *Phys. Rev. Lett.* 70:1315; see also A. D. Mirlin & Y. V. Fyodorov, *Europhys. Lett.* 25:669 (1994).

Fyodorov, Y. V., & D. V. Savin. 2004. Preprint, cond-mat/0409084; see also D. V. Savin & H.-J. Sommers, *Phys. Rev. E* 69:035201 (2004); D. V. Savin & H.-J. Sommers, *Phys. Rev. E* 68:036211 (2003).

Fyodorov, Y. V., & H. J. Sommers. 1997. *J. Math. Phys.* 38:1918.

Gutzwiller, M. C. 1990. *Chaos in classical and q uantum mechanics*. New York: Springer-Verlag.

Haake, F. 1991. *Quantum signatures of chaos*. New York: Springer-Verlag.

Heller, E. J. 1984. *Phys. Rev. Lett.* 53:1515.

Hemmady, S., X. Zheng, E. Ott, T. Antonsen, & S. Anlage. 2004. cond-mat/0403225, accepted by *Phys. Rev. Lett.*

Hill, D. A. 1994. *IEEE Trans. EMC* 36:294; see also 40:209 (1998); L. Cappetta, M. Feo, V. Fiumara, V. Pierro & I. M. Pinto. 1998. *IEEE Trans. EMC* 40:185 (1998).

Holland, R., & R. St. John. 1994. *Conference Proceedings: 10th Annual Review of Progress in Applied Computational Electromagnetics*, Monterey, CA, March, Vol. 2, pp. 554–568.

Holland, R., & R. St. John. 1999. *Statistical electromagnetics*. Philadelphia: Taylor & Francis.

Jalabert, R. A., A. D. Stone, & Y. Alhassid. 1992. *Phys. Rev. Lett.* 68:3468.

Kogan, E., P. A. Mello, & H. Liqun. 2000. *Phys. Rev. E.* 61:R17.

Kostas, J. G., & B. Boverie. 1991. *IEEE Trans. EMC* 33:366.

Krieger, T. J. 1967. *Ann. of Phys.* 42:375.

Kuhl, U., M. Martínez-Mares, R. A. Méndez-Sánchez, & H.-J. Stöckmann. cond-mat/0407197.

Lane, A. M., & R. G. Thomas. 1958. *Rev. Mod. Phys.* 30:257.

Lehman, T. H., & E. K. Miller. 1991. *Conference Proceedings: Progress in Electromagnetics Research Symposium*, Cambridge, MA, July 1–5, p. 428.

Lewenkopf, C. H., & H. A. Weidenmüller. 1991. *Ann. of Phys.* 212:53.

Mahaux, C., & H. A. Weidenmüller. 1969. *Shell-model approach to nuclear reactions*. Amsterdam: North-Holland.

Mehta, M. L. 1991. *Random matrices*, 2nd ed. New York: Academic Press; see also K. B. Efetov, *Adv. Phys.* 32:53 (1983).

Mello, P. A. 1995. In *Mesoscopic quantum physics*, ed. E. Akkermans, G. Montambaux, J. L. Pichard, & J. Zinn-Justin. Amsterdam: North Holland.

Mello, P. A., P. Peveyra, & T. H. Seligman. 1985. *Ann. of Phys.* 161:254; see also G. López, P. A. Mello, & T. H. Seligman, *Z. Phys. A* 302:351 (1981).

Méndez-Sánchez, R. A., U. Kuhl, M. Barth, C. H. Lewenkopf, & H.-J. Stöckmann. 2003. *Phys. Rev. Lett.* 91:174102.

Ott, E. 2002. *Chaos in dynamical systems*, 2nd ed. Cambridge, England: Cambridge University Press.

Price, R. H., H. T. Davis, & E. P. Wenaas. 1993. *Phys. Rev. E* 48:4716.

Taniguchi, N., & V. N. Prigodin. 1996. *Phys. Rev. B.* 54:14305.

Verbaarschot, J. J. M., H. A. Weidenmüller, & M. R. Zirnbauer. 1985. *Phys. Rep.* 129:367.

Warne, L. K., K. S. H. Lee, H. G. Hudson, W. A. Johnson, R. E. Jorgenson, & S. L. Stronach. 2003. *IEEE Trans. on Anten. and Prop.* 51:978.

Wigner, E. P. 1951. *Ann. Math.* 53:36; see also 62:548 (1955); 65:203 (1957); 67:325 (1958).

Wigner, E. P., & L. Eisenbud. 1947. *Phys. Rev.* 72:29.